Environmental Science & Technology

Article

pubs.acs.org/est

Heterogeneous Mercury Oxidation on Au(111) from First Principles

Dong-Hee Lim[†] and Jennifer Wilcox*[,‡]

[†]Fuel Cell Research Center, Korea Institute of Science and Technology (KIST), Hwarangno 14-gil 5, Seongbuk-gu, Seoul 136-791, Republic of Korea

[‡]Department of Energy Resources Engineering, Stanford University, 367 Panama Street, Green Earth Sciences, Stanford, California 94305-2220, United States

ABSTRACT: Density functional theory (DFT) studies of mercury oxidation on Au(111) are conducted to determine the potential Hg oxidation mechanisms taking place on catalytic gold surfaces by using the Perdew and Wang approximation (PW91) described by a generalized gradient approximation (GGA). The Hg oxidation was examined via a Langmuir–Hinshelwood mechanism where each Hg^0 and Cl_2 (or HCl) species is separately adsorbed on the gold surface and the bimolecular reaction occurs through the formation of bound HgCl and $HgCl_2$. For this, the Climbing Image-Nudged Elastic Band (CI-NEB) method has been employed to calculate the activation energies of HgCl and $HgCl_2$ formation pathways. In the three-step Hg oxidation mechanism (Hg → HgCl → $HgCl_2$), the second Cl attachment step is endothermic which is the reaction rate-limiting step, while the first Cl attachment step is exothermic. This observation implies that Hg oxidation prefers a pathway in which HgCl and $HgCl_2$ are formed, rather than a pathway directly oxidizing Hg to $HgCl_2$. In the presence of H atoms due to HCl dissociation on the Au surface, the H atoms lower the activation energy for Hg oxidation by consuming the electron charge of Au atoms, thereby weakening the strength of interaction between Cl and the Au surface and lowering an energy required to detach Cl from the Au surface. This mechanism is in the absence of site competition on the Au surface. In addition, details of the electronic properties of these systems are discussed.

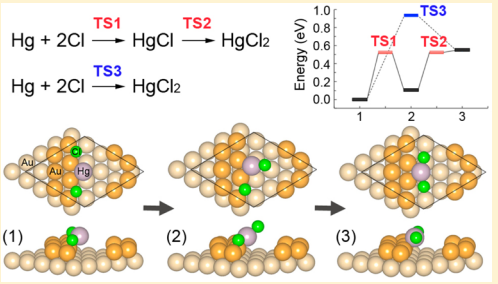

1. INTRODUCTION

The release of anthropogenic mercury (Hg) is of serious global concern, and its major emissions source is from coal-fired power plants.[1−3] Mercury is highly volatile and therefore exists almost exclusively in the vapor phase of combustion and gasification flue gases.[4,5] In coal-derived flue gas, it is known that Hg exists in three forms: elemental (Hg^0), oxidized (Hg^{2+}), and particle-bound (Hg_p).[2,4] Both Hg^{2+} and Hg_p are readily removed from the flue gas using wet flue gas desulfurization (FGD) units for Hg^{2+} and electrostatic precipitators for Hg_p.[2] However, it is difficult to capture Hg^0 due to its high vapor pressure and low solubility.[2,4] Activated carbon is currently used to remove Hg^0 and Hg^{2+}, and noble metals (gold (Au), platinum (Pt), palladium (Pd)) are also potential alternatives for Hg oxidation.[2,6,7] In particular, Au has been considered as a potential catalyst for Hg oxidation[2,6,7] because Au can be catalytically very active in the presence of highly under-coordinated Au atoms[8] or in the form of nanoparticles on suitable supports[9] such as TiO_2, SiO_2, Fe_2O_3, Al_2O_3, MgO, and ZnO.[10−12] In addition, pilot-scale tests[13] of Hg oxidation have suggested that the higher cost of precious metals (Au or Pd) can be offset by requiring less metal (44% less in volume) and a potential longer life compared to carbon-based sorbent catalysts.

The predominant and actual physicochemical forms of the elemental and inorganic Hg^{2+} phases are $Hg^0(g)$, $HgCl_2(g)$, HgO(s,g), and $HgSO_4(s)$.[4] The $HgCl_2(g)$ phase is dominant at temperatures less than about 450 °C and the relative proportion of HgO(g) is minor compared to $HgCl_2(g)$ and $Hg^0(g)$.[4] Considering the predominant HCl concentration compared to Cl_2 (~1% of the HCl concentration) in the flue gas, the overall reaction of the catalytic oxidation of Hg to $HgCl_2$ is assumed as Hg + 2HCl → $HgCl_2$.[7]

It has been known that Hg oxidation can occur via one of three possible Hg oxidation mechanisms:[7] a Langmuir–Hinshelwood mechanism, an Eley–Rideal mechanism, or a Mars-Maessen mechanism. According to the Langmuir–Hinshelwood mechanism,[14] each gas species (Hg^0 and Cl_2) is first separately adsorbed on a catalyst surface, the adsorbed species react and form an adsorbed product of $HgCl_2$, and the product is ultimately desorbed into the gas phase. In an Eley–Rideal mechanism,[15,16] one of two species (Hg^0 or Cl_2) is adsorbed while the other remains in the gas-phase, and they react with each other producing $HgCl_2$ in the gas phase. Lastly, in a Mars-Maessen mechanism[17] adsorbed Hg^0 reacts with a lattice oxidant (either Cl or O) that is replenished from the gas phase, and an adsorbed product, $HgCl_2$ or HgO, desorbs into the gas phase. In the case of the Pt catalyst, Presto and Granite[7] suggested that adsorbed Hg on the Pt catalyst may react with gas phase HCl in accordance with an Eley–Rideal mechanism based on experimental observation that Hg oxidation stops in

Received: February 26, 2013
Revised: June 17, 2013
Accepted: June 27, 2013
Published: June 27, 2013

   dx.doi.org/10.1021/es400876e | Environ. Sci. Technol. 2013, 47, 8515−8522

the absence of HCl.[7] To date, none of the three mechanisms has been verified as the dominant mechanism for catalytic Hg oxidation.[7]

From experimental observations, it appears that Hg reacts from an adsorbed state,[2] and it is also well-known that Hg adsorbs to Au, Pt, and Pd surfaces.[7] Presto and Granite[7] measured Hg oxidation on Au and Pd catalysts by exposing the catalysts to HCl and changing the HCl concentration up to zero. They observed that Hg oxidation continues on the catalysts in the absence of gas phase HCl but with a declining reaction rate. From this observation, they concluded that Hg reacts with HCl that is bound to the catalyst surface. They also assumed that surface-bound chlorine should be available for Hg oxidation on the Au and Pd surfaces, based on the fact that Cl_2 can chemisorb to Au surfaces[18] and HCl dissociatively adsorbs to Pt surfaces.[19] Other experimental studies of Hg oxidation in flue gas have also shown that Hg oxidation increases with increasing HCl content.[20−22] However, details of Hg oxidation mechanisms in the flue gas are not yet well understood.

The specific goal of the current study is to investigate the potential of catalytic oxidation of Hg^0 by Cl_2 and HCl using density functional theory (DFT) predictions. Based on the experimental observation of Hg oxidation on Au[7] as previously discussed, we examine Hg oxidation via a Langmuir−Hinshelwood mechanism where each Hg^0 and Cl_2 (or HCl) species is separately adsorbed on the Au surface and the bimolecular reaction occurs to form $HgCl_2$. In addition, details of the structural and electronic properties of these systems are discussed.

2. COMPUTATIONAL METHODOLOGY

Density functional theory calculations were performed using the Vienna *ab initio* Simulation Package (VASP).[23−26] Ultrasoft Vanderbilt pseudopotentials[27] are used to describe core orbitals, and electron exchange correlation functionals were calculated using the Perdew and Wang[28] approximation (PW91) described by a generalized gradient approximation (GGA). The PW91 exchange-correlation functional has been known to provide a better description of Au−Au binding than Perdew-Burke-Ernzerhof (PBE) and revised-PBE (RPBE) functionals in terms of the calculated cohesive energy and the surface energy.[29] A plane-wave expansion with a cutoff of 300 eV was employed with Methfessel and Paxton[30] Gaussian-smearing of order 2 with a width of 0.1 eV. Geometric relaxation was obtained with the conjugate-gradient (CG) algorithm until the total energy change upon two iterations of the electronic self-consistent loop was less than 10^{-4} eV. The Monkhorst-Pack[31] scheme was used for the k-point sampling. Using 16 × 16 × 16 k-point meshes, the lattice constant of bulk Au was determined as 4.181 Å, which is in reasonable agreement with the experimental measurement of 4.08 Å[32] with a relative error of 2.5%. The cohesive energy of bulk Au (i.e., the energy required to break the atoms of the solid into isolated atomic species) was 3.14 eV/atom. This cohesive energy is underestimated by a relative error of 16.2% compared to the experimental value of 3.81 eV/atom;[33] however, it is consistent with other previous DFT studies with reported cohesive energies of 3.20,[34] 3.15,[35] and 3.06[36] eV/atom.

The Au(111)−p(4×4) surfaces were used for Hg oxidation modeling and were represented as a four-layer slab with 16 atoms in each layer and a 21.7 Å-thick vacuum region to prevent interactions between periodic images (Figure 1). The Brillouin zone integration of the Au(111)−p(4×4) surface was

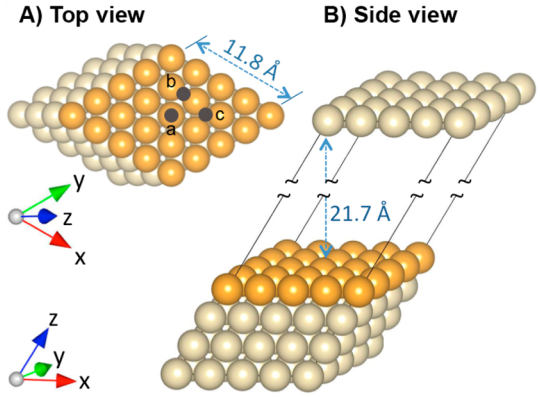

Figure 1. Perfect Au(111)−p(4×4) surface model: (A) top and (B) side views. Orange and light gray colors represent the top Au surface and the subsurface, respectively. a, b, and c indicate the adsorption sites of atop, bridge, and 3-fold, respectively.

calculated using 5 × 5 × 1 Monkhorst-Pack[31] k-point meshes. The xy-plane is parallel to the surface, and the z-axis is perpendicular to the surface. The bottom two layers were fixed at the equilibrium lattice constant of 4.181 Å and the top two layers were fully relaxed. In our previous Hg adsorption study on Au(111) surfaces where a cutoff energy of 350 eV was used,[37] the four-layer slab showed convergence of the surface energy within 1 meV/Å^2 compared to a 20-layer slab. It was also validated in the previous study that a dipole correction associated with the asymmetric slab and the spin-polarized correction had a negligible effect on the Hg adsorption energy on Au(111) surfaces[37] and therefore were not taken into account in the current study. Additional details of the validation of the DFT calculations are presented in our previous studies.[37,38]

The defective Au(111)−p(4×4) surfaces were modeled with a varying number of Au vacancies. The formation energy of n-vacancies on the Au(111) surface (E_{f_vac}) (i.e., an energy required to break the bond between atoms of the Au surface) was calculated from[39,40]

$$E_{f.vac} = E_{Au.vac} - E_{Ref} + nE_{bulk}$$

where n is the number of the vacancy, E_{Au_vac} is the total energy of Au(111) containing n-vacancies, E_{ref} is the total energy of Au(111) with no vacancy, and E_{bulk} is the total energy per Au atom in the bulk. The adsorption energies (E_{ads}) of adsorbates on defective Au(111)−p(4×4) surfaces are calculated as $E_{ads} = E_{Au+Adsorbate} - E_{Au} - E_{Adsorbate}$, where the three terms on the right-hand-side represent the total energy of the Au(111) surface with adsorbates, the total energy of the Au(111) surface, and the total energy of gas-phase adsorbates, respectively. With this definition of adsorption energy, the more negative the energy, the stronger the interaction.

The activation barriers for Hg oxidation are calculated using the climbing image nudged elastic band (CI-NEB) method that is known to effectively locate the minimum energy paths (MEPs) and the corresponding transition states of adsorbate molecules.[41] Once the initial and final configurations of a reaction path are known, intermediate configurations are determined by interpolating between the initial and final configurations. The interpolated chain of configurations is connected by springs and relaxed simultaneously to the MEP, through which the highest-energy configuration climbs uphill to the saddle point.[41]

dx.doi.org/10.1021/es400876e | Environ. Sci. Technol. 2013, 47, 8515−8522

3. RESULTS AND DISCUSSION

3.1. Perfect and Defective Au(111) Surface Models. The perfect four-layer Au(111)−p(4×4) slab has a rhombus-shaped surface with a side length of 11.8 Å, which consists of 16 Au atoms as shown in Figure 1. Among the adsorption sites of atop, bridge, and 3-fold in Figure 1A, the 3-fold site shows the most stable adsorption of atomic Hg and Cl atoms. The Hg (and Cl) adsorption energies at atop, bridge, and 3-fold sites of the perfect Au surface are −0.32 (−0.69), −0.40 (−0.98), and −0.43 (−0.99) eV, respectively. The most favorable adsorption configurations of Hg and Cl atoms give insight into the determination of the initial configurations of the reactants and products in the Hg oxidation pathways. More details of Hg adsorption behavior on the Au surfaces can be found in our previous study.[37]

The vacancy formation energies are compared in Figure 2 to determine a proper defective surface model of the Au surface

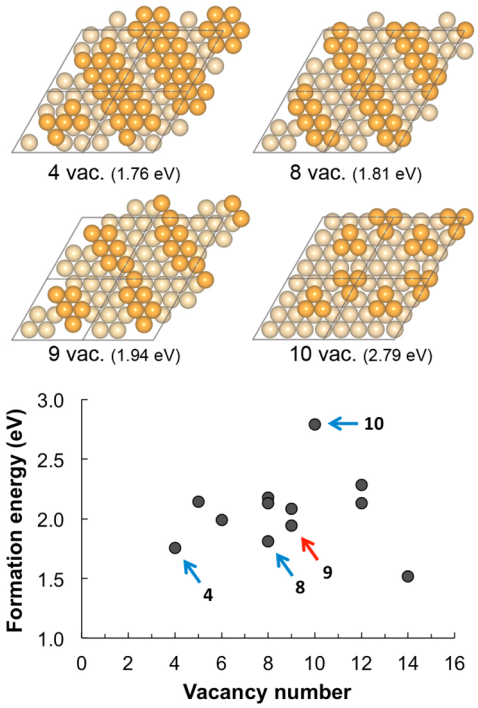

Figure 2. Defective Au(111)−p(4×4) surface models with vacancies (vac.) and the formation energies of n-vacancies (in parentheses) on the Au(111) surface (E_{f_vac}). The four rhombuses on the surface models represent (2×2) supercells of the Au(111)−p(4×4) surface. Orange and light gray colors represent the top Au surface and the 2nd Au subsurface, respectively. The third and fourth layers of Au are omitted.

for the Hg oxidation. Two criteria for the defective surface selection were the stability of the Au surface with vacancies in terms of the vacancy formation energy and the availability of the surface space for the mobility of adsorbates (Hg, Cl, and H). In Figure 2, the supercell of the Au(111)−p(4×4) is expanded to a (2×2) boundary for better visualization of the surface shape with periodic images. The 4-vacancy surface model has two closely packed steps, so that the product molecules of Hg oxidation (HgCl and $HgCl_2$) are readily stuck between the steps, leading to dispersed adsorption of the product components between the steps; the 14-vacancy surface model has the most favorable formation of the surface Au atoms but has too small of a surface for Hg oxidation to take place. Instead, the 9-vacancy surface model was chosen to have a large enough space between two steps, minimizing the interference of neighboring steps. The step sites promote the adsorption of atomic species; for example, the Hg and Cl adsorption energies at the step site of the 4-vacancy Au surface are −0.50 and −1.30 eV, respectively.

In Figure 2, the Au surfaces with continuous steps (4-, 8-, and 9-vacancy surface models) show more favorable formation requiring less energy to form vacancies, compared to the island-like surface (10-vacancy model). The continuous steplike Au surfaces are different from the well-known herringbone reconstruction of the Au(111) surface[42,43] where the top layer atoms are laterally compressed along the $[0\bar{1}1]$ direction and appear as lines approximately 0.2 Å higher than the surface (i.e., known as discommensuration lines);[44] however, the results shown in Figure 2 support a linear reconstruction of the Au(111) surface, rather than a dispersed islandlike surface reconstruction.

3.2. Hg Oxidation on Perfect Au(111) Surfaces. Prior to the Hg oxidation pathway analyses, it is necessary to determine the possible reactants, intermediates, and products in the Hg oxidation pathways. The initial configurations of the Hg oxidation species were estimated and optimized based on the most stable adsorption configurations of atomic Hg, Cl, and H atoms. Two Hg oxidation schemes were investigated: via the Cl_2 molecule (Cl_2 model) and via 2HCl molecules (HCl model). Three Hg oxidation steps for the Cl_2 model were taken into account on the Au(111) surfaces: 1) Hg + Cl + Cl, 2) HgCl + Cl, and 3) $HgCl_2$. For the HCl model, two atomic H atoms were added to each step assuming that HCl dissociatively adsorbs to the Au surface, as observed for HCl on Pt surfaces.[19] Figure 3 shows only one representative step for each Hg oxidation pathway model but gives to an overall picture how Hg oxidation proceeds since the geometry configurations of each step of the different oxidation schemes are similar except for the H atoms in the HCl models. At each initial oxidation step, atomic species are located at the 3-fold or bridge sites; at each second step, the HgCl molecule stands upright; at each third step, the $HgCl_2$ molecule is anchored with Hg bound and two Cl atoms turned upward.

Activation energies for Hg oxidation were calculated assuming two possible reaction pathways: three-step Hg oxidation (step 1 → 2 → 3) with transition states 1 and 2 (TS1 and TS2) and two-step Hg oxidation (step 1 → 3) with a transition state 3 (TS3) in Figure 3. When H atoms are absent (Figure 3A) and located far from the Hg and Cl atoms (Figure 3B), the three-step pathway is more favorable than the two-step pathway, showing lower activation energies. In the three-step pathway, the first Cl attachment is exothermic, but the second Cl attachment is endothermic (Table 1); in other words, the reaction rate-limiting step lies in the formation of $HgCl_2$ from HgCl. These theoretical observations lead to the conclusion that atomic Cl serves as a key role in oxidizing Hg by forming HgCl and $HgCl_2$ step by step, rather than oxidizing Hg directly to $HgCl_2$. This Hg oxidation trend agrees well with Zhao et al. experimental measurements of Hg oxidation with 3 ppm Cl_2 on gold where the rate constants (k at 473 K) of the reactions Hg→HgCl, HgCl→$HgCl_2$, and Hg→$HgCl_2$ are computed as 2.0×10^{17}, 8.0×10^{16}, and 1.0×10^{16}, respectively[6] (the rate constants are of the form $k = AT^n e^{-E/RT}$ where A is the pre-exponential factor ($cm^3/(mol/s)$), T is temperature (K), n is unitless, E is activation energy (kcal/mol), and R is the ideal gas

dx.doi.org/10.1021/es400876e | Environ. Sci. Technol. 2013, 47, 8515−8522

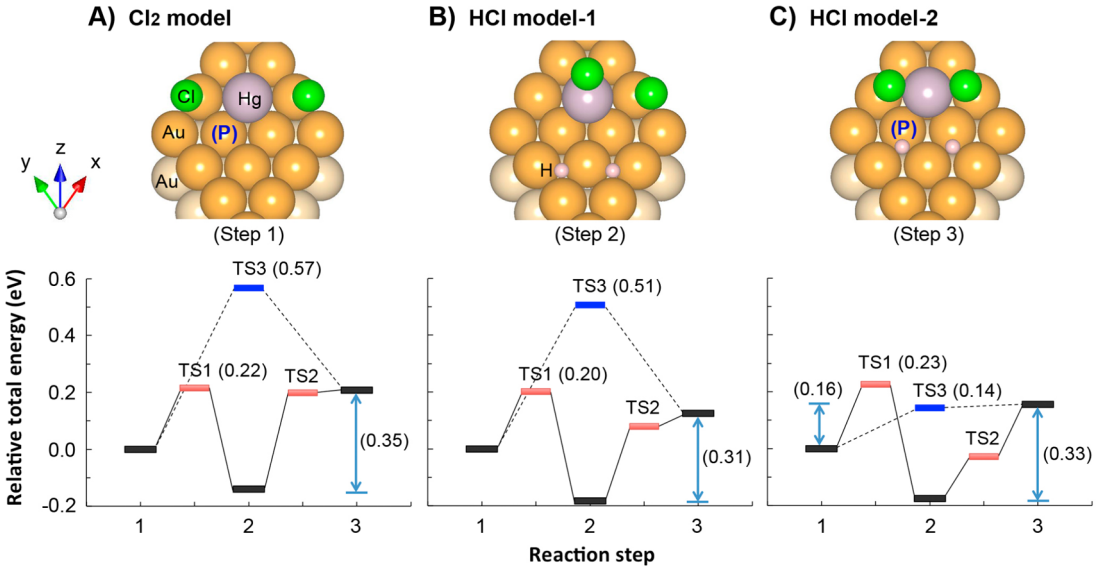

Figure 3. Reaction pathways of Hg oxidation on perfect Au(111)−p(4×4) surfaces via the Cl_2 molecule (A) and two HCl molecules (B and C depending on different H atom locations). Each model has three Hg oxidation steps (steps 1−3), but only one representative step is shown in parentheses for each model. TS1, 2, and 3 indicate transition states with activation energies in parentheses. TS1 and 2 (in red) are in a three-step Hg oxidation mechanism (step 1 → 2 → 3) and TS3 (in blue) is in a two-step Hg oxidation mechanism (step 1 → 3). Purple, green, white (small circle), orange, and light gray colors represent the Hg atom, Cl atom, H atom, top Au surface, and 2nd Au subsurface, respectively. The third and fourth layers of Au are omitted. **(P)** in blue indicates the Au atoms used for the projected density of states (PDOS) in Figure 4.

Table 1. Reaction Energy Barriers (in eV) for Hg Oxidation on Perfect and Defective Au(111)−p(4×4) with 9 Vacancies via the Cl_2 Molecule (Cl_2 Model) and 2HCl Molecules (HCl Model-1 and -2) According to Figures 3 and 5[a]

	perfect Au(111)			defective Au(111)		
	three-step pathway		two-step pathway	three-step pathway		two-step pathway
	step 1 → 2 (Hg→HgCl)	step 2 → 3 (HgCl→$HgCl_2$)	step 1 → 3 (Hg→$HgCl_2$)	step 1 → 2 (Hg→HgCl)	step 2 → 3 (HgCl→$HgCl_2$)	step 1 → 3 (Hg→$HgCl_2$)
Cl_2 model	0.22	0.35	0.57	0.52	0.45	0.94
HCl model-1	0.20	0.31	0.51	0.45	0.55	0.91
HCl model-2	0.23	0.33	0.16	0.22	0.27	0.62

[a]Numbers 1, 2, and 3 in the second row indicate three Hg oxidation steps of 1) Hg + Cl + Cl, 2) HgCl + Cl, and 3) $HgCl_2$, respectively.

constant (kcal/(mol·K))). Although our DFT activation energy was calculated for the ground state at 0 K, it ranges from 0.22 to 0.57 eV in the case of the Cl_2 model (Figure 3A) agreeing with the measurement of Zhao et al. with a reported apparent activation energy of 0.31 eV (7.2 kcal/mol) for the global reaction of $Hg^0 + Cl_2 \rightarrow HgCl_2$ on gold at 473 K.[6]

In the presence of H atoms attributed to HCl dissociation on gold (Figure 3B and 3C), the Hg oxidation reaction pathway is affected, altering the magnitude of the activation energies. The closer the H atoms are to the Hg oxidation intermediates, the greater influence the H atoms have on the reaction pathway. In Figure 3B where the H atoms are relatively far from the reaction intermediates, the activation energies are slightly lower compared to those of the Cl_2 model (Figure 3A). However, when the H atoms are relatively closer to the intermediates (Figure 3C), they significantly alter the activation energy of TS3 (0.14 eV for $Hg + Cl_2 \rightarrow HgCl_2$). It should be noted though that this extreme case of Figure 3C is one of many possible Hg oxidation pathways when the H atoms are closely placed near the reaction intermediates. Despite the difference in the magnitude of activation energy in the presence of H atoms, the H atom serves as an 'impurity' on the gold surface that consumes the electron charge of the gold atoms thereby lowering the strength of interaction between the gold atoms and the reaction intermediates, which ultimately enhances the Hg oxidation reaction by lowering the activation energy required to detach Cl atoms from the gold surface for the formation of HgCl and $HgCl_2$ species. Presto and Granite[7] measured an apparent activation energy of 0.41 eV (9.6 kcal/mol) for the global reaction of $Hg^0 + 2HCl \rightarrow HgCl_2$ on gold over temperatures ranging from 411 to 433 K, which agrees with our DFT activation energies ranging from 0.16 to 0.51 eV.

To understand in greater detail the role of the H atoms, the projected density of states (PDOS) of the gold atoms adjacent to the Hg atoms were analyzed by decomposing the electron density and wave function into the atomic orbital contributions. The PDOS of the Au surface atom adjacent to adsorbed Hg on each model marked as **(P)** in Figure 3A and 3C was analyzed as shown in Figure 4. Figure 4A and 4B represent the Au s-, p-, and d-orbitals of the Cl_2 model and HCl model-2, respectively. In the presence of H atoms in Figure 4B, the Au s-, p-, and d-orbitals are strongly hybridized with the H s-orbital and shifted to the lower energy level. In particular, the Au s-orbital significantly interacts with the H s-orbital as shown by the orbital overlap between approximately −7 and −9 eV in Figure 4B. This strong orbital hybridization between the Au and H orbitals stabilizes adsorption of the H atom on the Au surface, resulting in reducing the Au electron charge available for the

dx.doi.org/10.1021/es400876e | Environ. Sci. Technol. 2013, 47, 8515−8522

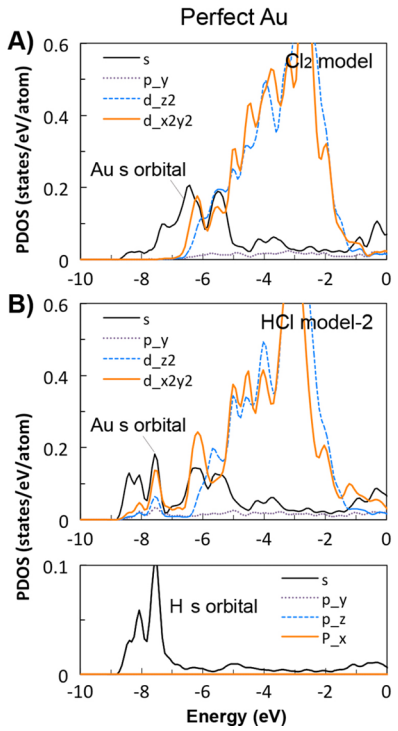

Figure 4. Projected density of states (PDOS) of the Au surface atoms adjacent to adsorbed Hg atoms on perfect Au(111)−p(4×4) surfaces (marked as (**P**) in Figure 3): Cl_2 model (A) and HCl model-2 (B). The Fermi energy is referenced at 0 eV.

reaction intermediates and relatively weakening the interactions between the intermediates and the Au surface. The weakened adsorption of the intermediates on the Au surface in turn lowers the activation energy for Hg oxidation, which ultimately promotes Hg oxidation. In addition, the d-band centers (relative to the Fermi level) of Figures 4A and 4B are −3.25 and −3.40 eV, respectively. It is known that the higher shift of the d-band center toward the Fermi level indicates the higher reactivity of a transition metal resulting in an increase in the stability of adsorbates.[45] The d-band center shifts downward relative to the Fermi level from Figures 4A to 4B due to the H atoms, which supports the relatively weakened adsorption of the intermediates on the HCl model-2 compared to on the Cl_2 model.

3.3. Hg Oxidation on Defective Au(111) Surfaces. The same Hg oxidation pathways examined on perfect Au(111)−p(4×4) surfaces were investigated on the Au surface with 9 vacancies as shown in Figure 5; two Hg oxidation schemes (Cl_2 model and HCl model), three and two oxidation steps for each model, and different H atom locations for the HCl model were considered. Figure 5 shows only one representative step for each Hg oxidation pathway model where the reaction intermediate species are adsorbed at the edge of the step. Activation energies for Hg oxidation were calculated according to the three-step (TS1 and TS2) and two-step (TS3) reactions.

Compared to the perfect Au surfaces, the defective Au surfaces become more reactive in terms of adsorption strength due to the defect sites, making it more difficult for Hg to be oxidized. The defective Au surfaces show approximately two times higher activation energy on average (Table 1), except for the HCl model-2 case, in which the H atom strongly interferes with the interaction between the intermediates and the Au surface. This trend is attributed to the stronger interactions of adsorbate species (Hg and Cl atoms) on the step site of the defective Au surface compared to the surface of perfect Au since the relatively stronger binding of the adsorbate species requires higher energy to be detached from the surface for Hg oxidation. A similar phenomenon has been reported in the case of the oxygen reduction reaction (ORR) on platinum (Pt) nanoparticles, indicating that stronger oxygen binding on Pt nanoparticle surfaces requires higher energy barriers for the ORR.[46] The Cl adsorption energies on the perfect Au surface,

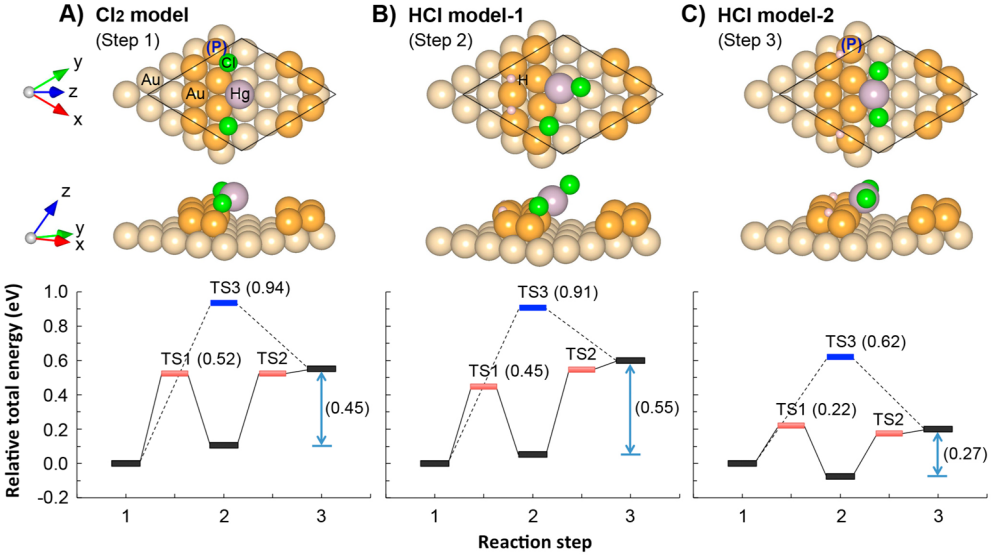

Figure 5. Reaction pathways of Hg oxidation on defective Au(111)−p(4×4) surfaces with 9 vacancies via Cl_2 molecule (A) and two HCl molecules (B and C depending on different H atom locations). Each model has three Hg oxidation steps (steps 1−3), but only one representative step is shown in parentheses at each model. TS1, 2, and 3 indicate transition states with activation energies in parentheses. TS1 and 2 (in red) are in a three-step Hg oxidation (step 1 → 2 → 3), and TS3 (in blue) is in a two-step Hg oxidation (step 1 → 3). Purple, green, white (small circle), orange, and light gray colors represent Hg atom, Cl atom, H atom, the top Au surface, and the 2nd Au subsurface, respectively. The third and fourth layers of Au are omitted. (**P**) in blue indicates the Au atoms used for the projected density of states (PDOS) in Figure 6.

dx.doi.org/10.1021/es400876e | Environ. Sci. Technol. 2013, 47, 8515−8522

for example, range from −0.69 to −0.99 eV, while showing −1.30 eV at the step site of a defective Au surface with 4 Au atom vacancies.

As concluded from the Hg oxidation pathways on perfect Au surfaces, the Hg reaction pathways on defective Au surfaces also indicate an important role of atomic Cl in Hg oxidation, leading to a step-by-step Hg oxidation (Hg → HgCl → $HgCl_2$) rather than directly from Hg to $HgCl_2$. In addition, the H atoms adjacent to the reaction intermediates promote the Hg oxidation by weakening the interaction between the Au surface and intermediates as discussed in Section 3.2.

An interesting comparison between the current theoretical calculations and Zhao et al. experimental observations[6] lies in the effect of HCl on Hg oxidation. Zhao et al. measured Hg oxidation by separately applying 50 ppm HCl and 3 ppm Cl_2 at 473 K and reported that the reduction percentages of inlet Hg were approximately 5 and 50% for the HCl and Cl_2 conditions, respectively. In a combination of the two gas conditions, the Hg reduction percentage was even reduced to approximately 40%. This observation implies that HCl has relatively weaker oxidizing capability compared to Cl_2 and competes with Cl_2 for the active sites.[6] It seems that Zhao et al. experimental results are contrary to the current DFT results showing enhanced Hg oxidation in the HCl models. It is important to recognize that the HCl model used in the current study (Figure 3 and 5) is not a gold surface exposed to HCl gas but rather a gold surface containing adsorbed H and Cl atoms. In the current DFT simulation it was assumed that HCl is first dissociated on gold prior to Hg oxidation, based on the fact that HCl dissociatively adsorbs to Pt surfaces.[19] Due to this difference, the H atoms in the DFT simulations serve as "impurities" that weaken the adsorption energies of Hg and Cl atoms on the Au surface thereby lowering the activation energies for combining Hg and Cl atoms, which ultimately enhances Hg oxidation. Furthermore, as discussed in the Introduction, the HCl molecule interacts with Hg in a bound form on the Au surface in the Hg oxidation mechanism, rather than as gas phase HCl.[7] Also, the current DFT results suggest that the dissociated H atoms from HCl molecules help oxidize Hg and the experimental observations support relatively weaker oxidizing capability of HCl compared to Cl_2. Considering all of these findings, it may be suggested that HCl molecules may be bound on the Au surface in a configuration in which the Cl atoms are directly adsorbed on gold with H directed toward the gas phase, in which the H atoms may not be dissociated prior to Hg oxidation. Another possible interpretation for the discrepancy may lie in the difference in the surface area between the experimental conditions and the pure computational environment. Considering the higher concentration of HCl (50 ppm) compared to Cl_2 (3 ppm) in Zhao et al. experiment conditions, if the gold surface area is relatively small, H and Cl atoms and HCl molecules may compete with one another for active sites, resulting in lower Hg oxidation by HCl compared to Cl_2. On the other hand, the current DFT modeling environment provides no competition effect (no coverage effect) for the active sites between H and Cl atoms.

Figure 6 shows the PDOS of the Au surface atom adjacent to the adsorbed Hg atom on each defective Au model marked as (**P**) in Figures 5A and 5C. Figures 6A and 6B represent the Au *s*-, *p*-, and *d*-orbitals of the Cl_2 model and HCl model-2, respectively. As discussed in the PDOS of the perfect Au models in Figure 4, when the H atoms are present, the Au *s*-, *p*-, and *d*-orbitals are strongly hybridized with the H *s*-orbital and

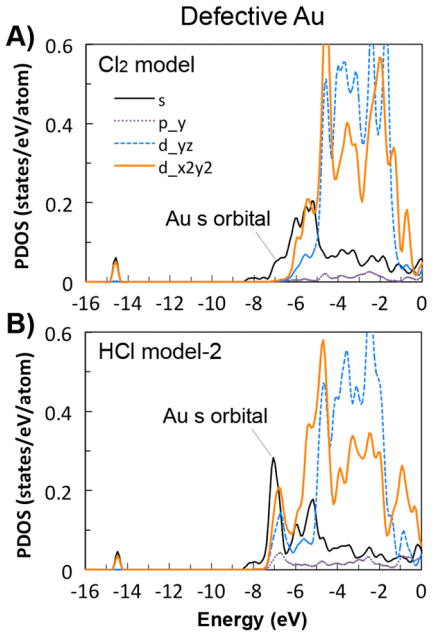

Figure 6. Projected density of states (PDOS) of the Au surface atoms adjacent to adsorbed Hg atoms on defective Au(111)−p(4×4) surfaces with 9 vacancies (marked as (**P**) in Figure 5): Cl_2 model (A) and HCl model-2 (B). The Fermi energy is referenced at 0 eV.

shifted to the lower energy level, especially between approximately −6 and −8 eV in Figure 6B. This significant interaction between the Au and H atoms weakens the interaction between the Au surface and the Hg intermediates and in turn lowers the activation energy for Hg oxidation, which ultimately promotes Hg oxidation. The *d*-band centers of Figures 6A and 6B (−3.02 and −3.25 eV, respectively) also support the relatively weakened interaction of the intermediates on the HCl model-2 compared to the Cl_2 model. In addition, due to the presence of the H atoms, the overall *d*-band center shifts of the perfect model (−3.25 to −3.40 eV) and the defective model (−3.02 to −3.25 eV) indicate that the defective surface has higher reactivity in terms of adsorbate stability, but this higher stability hinders Hg from being oxidized to HgCl and $HgCl_2$.

For environmental technology implications, the current DFT work provides insight into the Hg oxidation mechanism on gold, which will be used for the design of effective Hg control technologies. For example, it will be indispensable for promoting Hg oxidation to recognize that a balance in Hg adsorption stability on gold may be necessary to provide stable binding of Hg on gold while still maintaining weak binding of Hg oxidizing species for release into the gas phase. This balance may, for example, be applied by controlling the degree of defect sites on gold as well as precovering gold surfaces with atomic S or O species.[37]

For future studies, it may be of interest to use DFT modeling to investigate the effects of real flue gases that include trace species such as SO_2, NO, O_2, and H_2O and to investigate the impact of catalyst supports on mercury oxidation. In addition, similar DFT modeling studies of the current work on Pd and Pt surfaces may provide further insight into the Hg oxidation since Pd and Pt metals are also of commercial interest.

dx.doi.org/10.1021/es400876e | *Environ. Sci. Technol.* 2013, 47, 8515−8522

AUTHOR INFORMATION

Corresponding Author

*Phone: 650-724-9449. Fax: 650-725-2099. E-mail: wilcoxj@stanford.edu.

Notes

The authors declare no competing financial interest.

ACKNOWLEDGMENTS

We thank the Electric Power Research Institute for making this research possible through their mercury research funding to the Clean Energy Conversions Laboratory at Stanford University. The computational resources were supported by the National Science Foundation through TeraGrid resources provided by Texas Advanced Computing Center (TACC) and in part by the supercomputing cluster of the Center for Computational Earth & Environmental Science at Stanford University. The current work is also supported by Basic Science Research Program through the National Research Foundation (NRF) of Korea funded by the Ministry of Education, Science and Technology (NRF-2012R1A6A3A04040490).

REFERENCES

(1) Wilcox, J.; Rupp, E.; Ying, S. C.; Lim, D. H.; Negreira, A. S.; Kirchofer, A.; Feng, F.; Lee, K. Mercury adsorption and oxidation in coal combustion and gasification processes. *Int. J. Coal Geol.* **2012**, *90–91*, 4–20.

(2) Presto, A. A.; Granite, E. J. Survey of catalysts for oxidation of mercury in flue gas. *Environ. Sci. Technol.* **2006**, *40* (18), 5601–5609.

(3) Presto, A. A.; Granite, E. J.; Karash, A.; Hargis, R. A.; O'Dowd, W. J.; Pennline, H. W. A kinetic approach to the catalytic oxidation of mercury in flue gas. *Energy Fuels* **2006**, *20* (5), 1941–1945.

(4) Galbreath, K. C.; Zygarlicke, C. J. Mercury speciation in coal combustion and gasification flue gases. *Environ. Sci. Technol.* **1996**, *30* (8), 2421–2426.

(5) Otani, Y.; Emi, H.; Kanaoka, C.; Matsui, S. Behavior of metal mercury in gases. *Environ. Sci. Technol.* **1984**, *18* (10), 793–796.

(6) Zhao, Y. X.; Mann, M. D.; Pavlish, J. H.; Mibeck, B. A. F.; Dunham, G. E.; Olson, E. S. Application of gold catalyst for mercury oxidation by chlorine. *Environ. Sci. Technol.* **2006**, *40* (5), 1603–1608.

(7) Presto, A. A.; Granite, E. J. Noble metal catalysts for mercury oxidation in utility flue gas: gold, palladium and platinum formulations. *Platinum Met. Rev.* **2008**, *52* (3), 144–154.

(8) Biener, M. M.; Biener, J.; Friend, C. M. Enhanced transient reactivity of an O-sputtered Au(111) surface. *Surf. Sci.* **2005**, *590* (2–3), L259–L265.

(9) Biener, J.; Biener, M. M.; Nowitzki, T.; Hamza, A. V.; Friend, C. M.; Zielasek, V.; Baumer, M. On the role of oxygen in stabilizing low-coordinated au atoms. *ChemPhysChem* **2006**, *7* (9), 1906–1908.

(10) Rodriguez, J. A.; Liu, P.; Vines, F.; Illas, F.; Takahashi, Y.; Nakamura, K. Dissociation of SO_2 on Au/TiC(001): Effects of Au-C interactions and charge polarization. *Angew. Chem., Int. Ed.* **2008**, *47* (35), 6685–6689.

(11) Lin, S. D.; Bollinger, M.; Vannice, M. A. Low-temperature CO oxidation over Au/TiO_2 and Au/SiO_2 catalysts. *Catal. Lett.* **1993**, *17* (3–4), 245–262.

(12) Haruta, M. Size- and support-dependency in the catalysis of gold. *Catal. Today* **1997**, *36* (1), 153–166.

(13) Blythe, G.; Dombrowski, K.; Machalek, T.; Richardson, C.; Richardson, M. *Pilot Testing of Mercury Oxidation Catalysts for Upstream of Wet FGD Systems, Final Report*; Cooperative Agreement DE-FC26-01NT41185; EPRI: Palo Alto, CA, U.S. Department of Energy, National Energy Technology Laboratory: Pittsburgh, PA, October 2006.

(14) Pilling, M. J.; Seakins, P. W. *Reaction Kinetics*; Oxford University Press: Oxford, U.K., 1995.

(15) Niksa, S.; Fujiwara, N. Predicting extents of mercury oxidation in coal-derived flue gases. *J. Air Waste Manage. Assoc.* **2005**, *55* (7), 930–939.

(16) Niksa, S.; Fujiwara, N. A predictive mechanism for mercury oxidation on selective catalytic reduction catalysts under coal-derived flue gas. *J. Air Waste Manage. Assoc.* **2005**, *55* (12), 1866–1875.

(17) Granite, E. J.; Pennline, H. W.; Hargis, R. A. Novel sorbents for mercury removal from flue gas. *Ind. Eng. Chem. Res.* **2000**, *39* (4), 1020–1029.

(18) Spencer, N. D.; Lambert, R. M. Chlorine chemisorption and surface chloride formation on Au(111). *Surf. Sci.* **1981**, *107* (1), 237–248.

(19) Wagner, F. T.; Moylan, T. E. Hydrogen-chloride adsorption and coadsorption with hydrogen or water on platinum(111). *Surf. Sci.* **1989**, *216* (3), 361–385.

(20) Senior, C. L. Oxidation of mercury across selective catalytic reduction catalysts in coal-fired power plants. *J. Air Waste Manage. Assoc.* **2006**, *56* (1), 23–31.

(21) Zhuang, Y.; Laumb, J.; Liggett, R.; Holmes, M.; Pavlish, J. Impacts of acid gases on mercury oxidation across SCR catalyst. *Fuel Process. Technol.* **2007**, *88* (10), 929–934.

(22) Eswaran, S.; Stenger, H. G. Effect of halogens on mercury conversion in SCR catalysts. *Fuel Process. Technol.* **2008**, *89* (11), 1153–1159.

(23) Kresse, G.; Hafner, J. Ab initio molecular dynamics for liquid metals. *Phys. Rev. B* **1993**, *47* (1), 558–561.

(24) Kresse, G.; Hafner, J. Ab initio molecular-dynamics simulation of the liquid-metal–amorphous-semiconductor transition in germanium. *Phys. Rev. B* **1994**, *49* (20), 14251–14269.

(25) Kresse, G.; Furthmüller, J. Efficient iterative schemes for ab initio total-energy calculations using a plane-wave basis set. *Phys. Rev. B* **1996**, *54* (16), 11169–11186.

(26) Kresse, G.; Furthmüller, J. Efficiency of ab-initio total energy calculations for metals and semiconductors using a plane-wave basis set. *Comput. Mater. Sci.* **1996**, *6* (1), 15–50.

(27) Vanderbilt, D. Soft self-consistent pseudopotentials in a generalized eigenvalue formalism. *Phys. Rev. B* **1990**, *41* (11), 7892.

(28) Perdew, J. P.; Wang, Y. Accurate and simple analytic representation of the electron-gas correlation energy. *Phys. Rev. B* **1992**, *45* (23), 13244.

(29) Baker, T. A.; Friend, C. M.; Kaxiras, E. Effects of chlorine and oxygen coverage on the structure of the Au(111) surface. *J. Chem. Phys.* **2009**, *130* (8), 084701.

(30) Methfessel, M.; Paxton, A. T. High-precision sampling for Brillouin-zone integration in metals. *Phys. Rev. B* **1989**, *40* (6), 3616–3621.

(31) Monkhorst, H. J.; Pack, J. D. Special points for Brillouin-zone integrations. *Phys. Rev. B* **1976**, *13* (12), 5188–5192.

(32) Pearson, W. B. *Handbook of Lattice Spacings and Structures of Metals and Alloys*; Pergamon Press: New York, 1967; Vol. *2*.

(33) Kittel, C. *Introduction to Solid State Physics*, 8th ed.; John Wiley & Sons, Inc.: New York, 2005.

(34) Yourdshahyan, Y.; Rappe, A. M. Structure and energetics of alkanethiol adsorption on the Au(111) surface. *J. Chem. Phys.* **2002**, *117* (2), 825–833.

(35) Grönbeck, H.; Curioni, A.; Andreoni, W. Thiols and disulfides on the Au(111) surface: The headgroup-gold interaction. *J. Am. Chem. Soc.* **2000**, *122* (16), 3839–3842.

(36) Hayashi, T.; Morikawa, Y.; Nozoye, H. Adsorption state of dimethyl disulfide on Au(111): Evidence for adsorption as thiolate at the bridge site. *J. Chem. Phys.* **2001**, *114* (17), 7615–7621.

(37) Lim, D.-H.; Aboud, S.; Wilcox, J. Investigation of adsorption behavior of mercury on Au(111) from first principles. *Environ. Sci. Technol.* **2012**, *46* (13), 7260–7266.

(38) Sasmaz, E.; Aboud, S.; Wilcox, J. Hg binding on Pd binary alloys and overlays. *J. Phys. Chem. C* **2009**, *113* (18), 7813–7820.

(39) Akbarzadeh, A. R.; Chen, Z. Z.; Kioussis, N. Crucial role of surface in stability and mobility of vacancy clusters in metals. *Phys. Rev. B* **2009**, *79* (19), 195404.

(40) Kiejna, A. Vacancy formation and O adsorption at the Al(111) surface. *Phys. Rev. B* **2003**, *68* (23), 235405.
(41) Henkelman, G.; Uberuaga, B. P.; Jonsson, H. A climbing image nudged elastic band method for finding saddle points and minimum energy paths. *J. Chem. Phys.* **2000**, *113* (22), 9901−9904.
(42) Chen, W.; Madhavan, V.; Jamneala, T.; Crommie, M. F. Scanning tunneling microscopy observation of an electronic superlattice at the surface of clean gold. *Phys. Rev. Lett.* **1998**, *80* (7), 1469−1472.
(43) Battaglini, N.; Repain, V.; Lang, P.; Horowitz, G.; Rousset, S. Self-assembly of an octanethiol monolayer on a gold-stepped surface. *Langmuir* **2008**, *24* (5), 2042−2050.
(44) Guo, Q. M.; Yin, F.; Palmer, R. E. Beyond the herringbone reconstruction: magic gold fingers. *Small* **2005**, *1* (1), 76−79.
(45) Hammer, B.; Nørskov, J. K. Electronic factors determining the reactivity of metal surfaces. *Surf. Sci.* **1995**, *343* (3), 211−220.
(46) Lim, D.-H.; Wilcox, J. Mechanisms of the oxygen reduction reaction on defective graphene-supported Pt nanoparticles from first-principles. *J. Phys. Chem. C* **2012**, *116*, 3653−3660.